



---

## Figures and figure supplements

The glycosphingolipid MacCer promotes synaptic bouton formation in *Drosophila* by interacting with Wnt

**Yan Huang *et al***

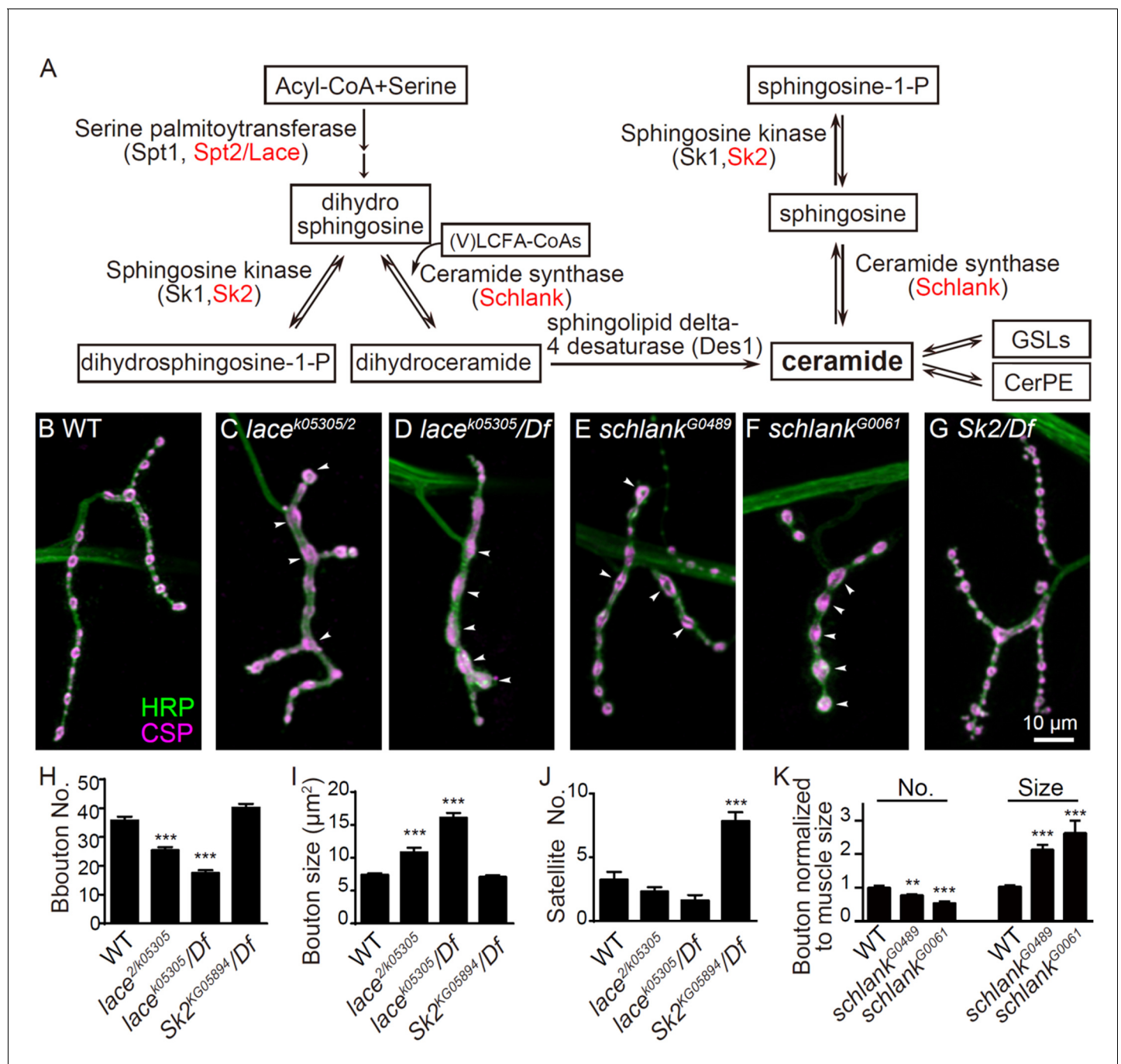


**Figure 1.** NMJ growth depends on de novo synthesis of ceramides (A) Simplified de novo biosynthesis pathway of sphingolipid in *Drosophila* is shown. (B–G) Representative images of NMJ4 co-stained with anti-HRP (green) and anti-CSP (magenta) in wild type (B), *lace<sup>k05305</sup>/lace<sup>2</sup>* (C), *lace<sup>k05305</sup>/Df* (2L)Exel7063 (D), *schlank<sup>G0489</sup>/Y* (E), *schlank<sup>G0061</sup>/Y* (F) and *Sk2<sup>KG05894</sup>/Df*(3L)BSC671 (G). Scale bar: 10  $\mu$ m; Arrowheads indicate large boutons in different mutants. (H–J) Quantifications of bouton number (H), bouton size (I) and satellite bouton number (J) of NMJs in abdominal segments A3 or A4 of different genotypes. (K) Bouton number and size in *schlank* mutants were normalized to muscle surface area as *schlank* mutants showed decreased body size (Bauer et al., 2009). \* $p < 0.05$ ; \*\* $p < 0.01$ , and \*\*\* $p < 0.001$  by student's *t* test between a test genotype and the wild-type control;  $n \geq 10$  larvae; error bars: s.e.m. Source data 1. Numerical data for the statistical graphs. The following figure supplement is available for Figure 1.

DOI: <https://doi.org/10.7554/eLife.38183.002>

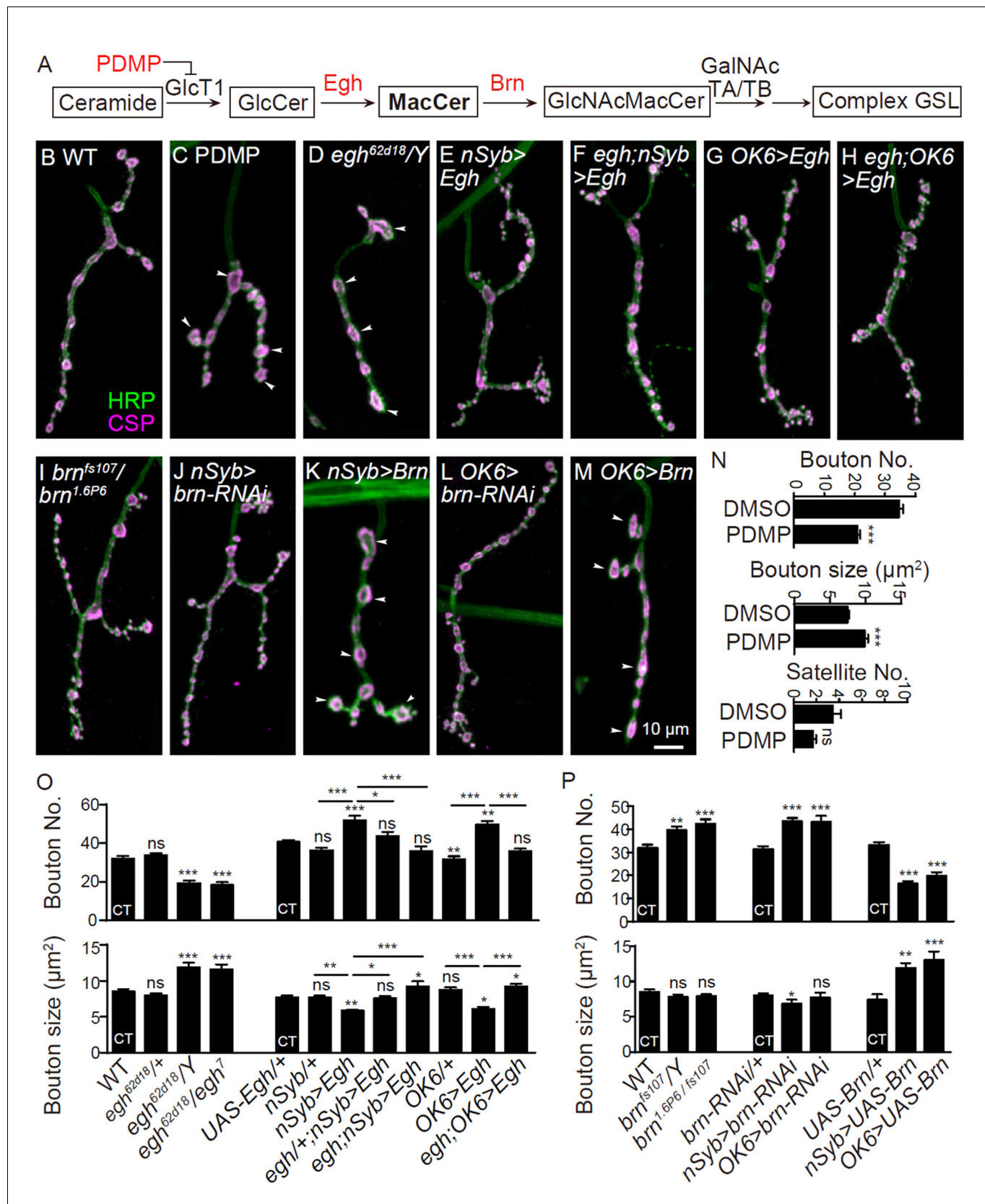


**Figure 2.** GSL synthases *Egh* and *Brn* bi-directionally regulates NMJ growth presynaptically (A) GSL synthesis pathway in *Drosophila*. (B–M) Images of NMJ4 co-stained with anti-HRP (green) and anti-CSP (magenta) in wild type (B), larvae treated with 0.5 mg/ml D, L-threo-PDMP (C), *egh*<sup>62d18</sup>/Y (D), UAS-

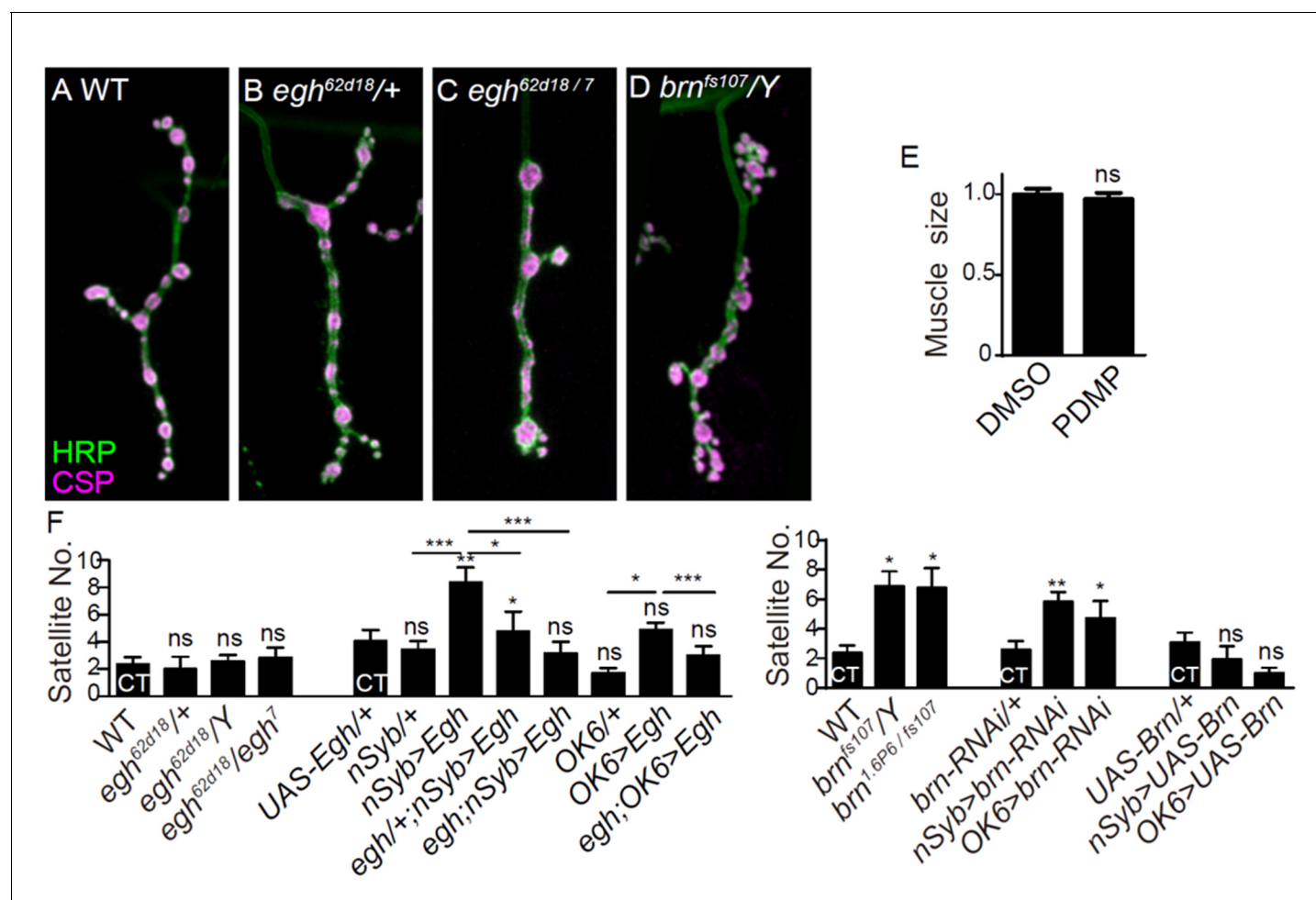
Figure 2 continued on next page

## Figure 2 continued

*Egh/+; nSyb-Gal4/+* (E), *egh<sup>62d18</sup>/Y; UAS-Egh/+; nSyb-Gal4/+* (F), *UAS-Egh/OK6-Gal4* (G), *egh<sup>62d18</sup>/Y; UAS-Egh/OK6-Gal4* (H) *brn<sup>fs107</sup>/brn<sup>1.6P6</sup>* (I), *UAS-brn-RNAi/+; nSyb-Gal4/+* (J) *nSyb-Gal4/UAS-brn* (K), *UAS-brn-RNAi/OK6 Gal4* (L), and *OK6-Gal4/+; UAS-brn/+* (M). Scale bar: 10  $\mu$ m; Arrowheads point at large boutons. (N–P) Quantifications of total bouton number, bouton size, and satellite bouton number of NMJs in different genotypes or treated with PDMP. 'CT' denotes corresponding control in each multiple comparison. \* $p < 0.05$ ; \*\* $p < 0.01$ , \*\*\* $p < 0.001$  by one-way ANOVA with Tukey *post hoc* tests;  $n \geq 12$  larvae; error bars: s.e.m.

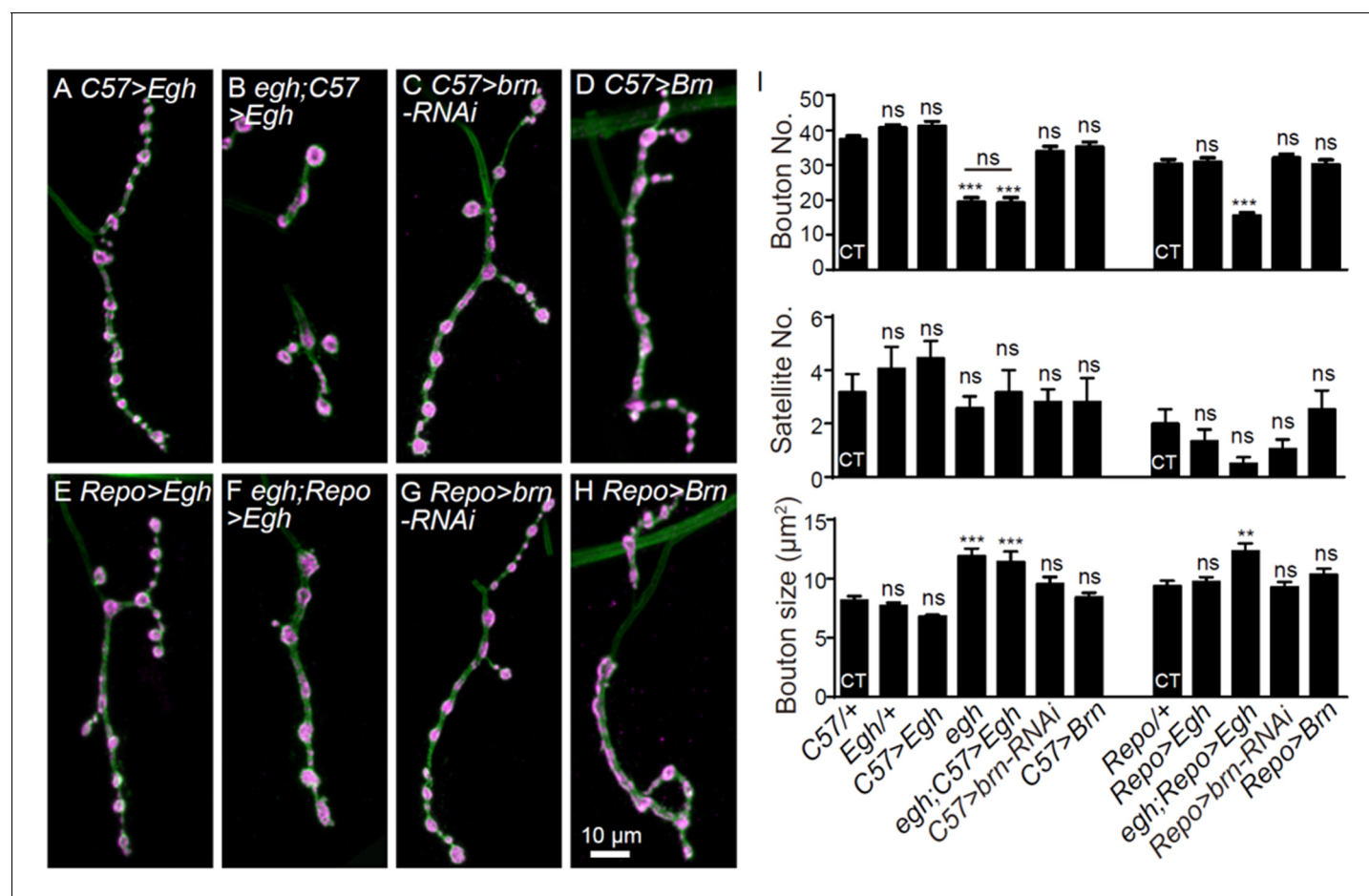
DOI: <https://doi.org/10.7554/eLife.38183.003>





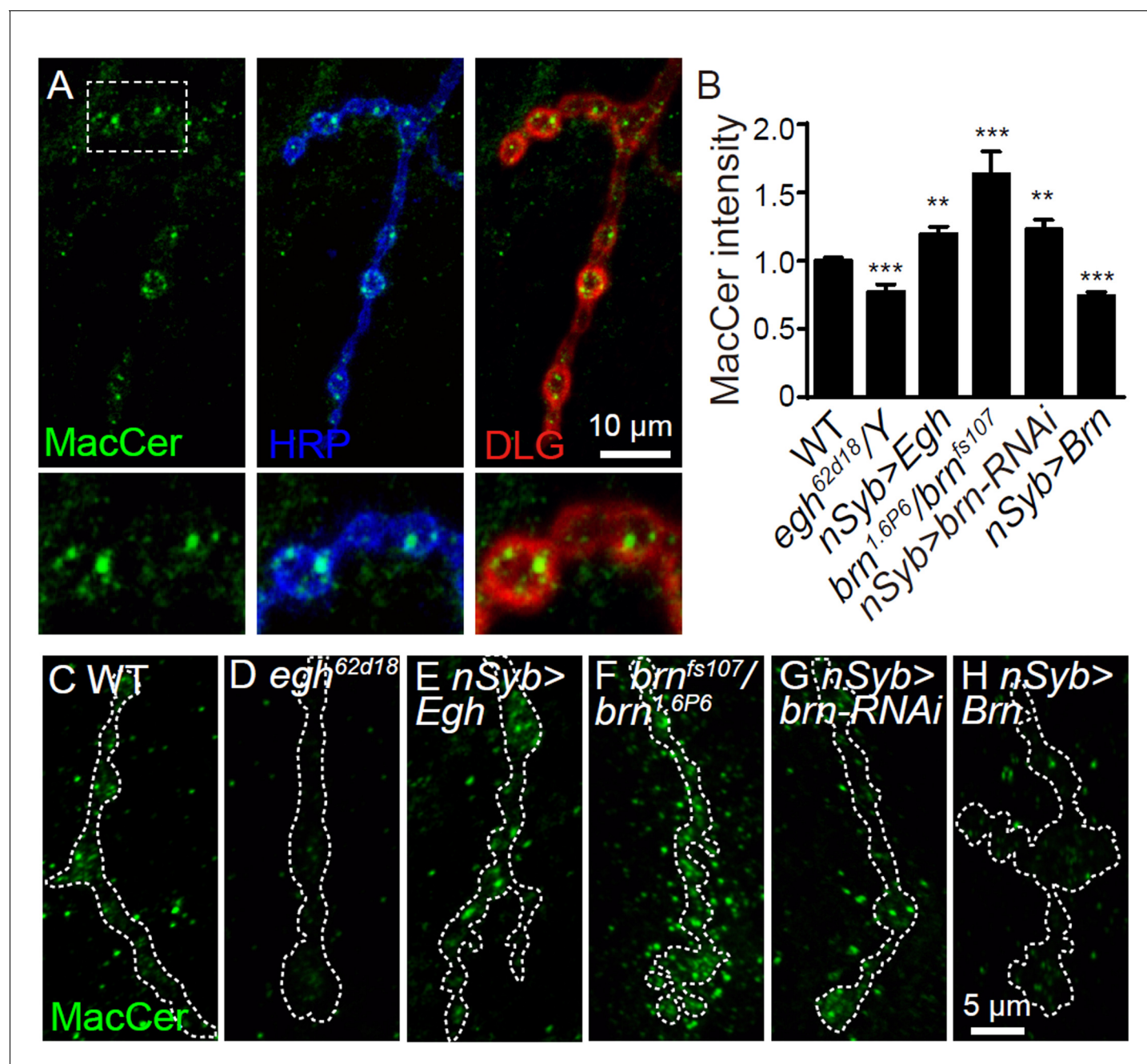
**Figure 2—figure supplement 1.** Additional NMJ images and quantifications. (A–D) Images of NMJ4 co-stained with anti-HRP (green) and anti-CSP (magenta) in wild type (A), *egh*<sup>62d18/+</sup> (B), *egh*<sup>62d18/egh</sup><sup>7</sup> (C), *brn*<sup>fs107/Y</sup> (D). Scale bar: 10  $\mu$ m. (E) Quantifications of muscle four surface area from wild type with or without D, L-threo-PDMP treatment at 0.5 mg/ml. ns, no significance, one-way ANOVA with Tukey *post hoc* tests;  $n \geq 8$  larvae; error bars: s.e.m. (F) Quantifications of satellite bouton number of NMJ4 from different genotypes. ns, no significance, \* $p < 0.05$ , \*\* $p < 0.01$ , \*\*\* $p < 0.001$  one-way ANOVA with Tukey *post hoc* tests;  $n \geq 12$ ; error bars: s.e.m.

DOI: <https://doi.org/10.7554/eLife.38183.004>



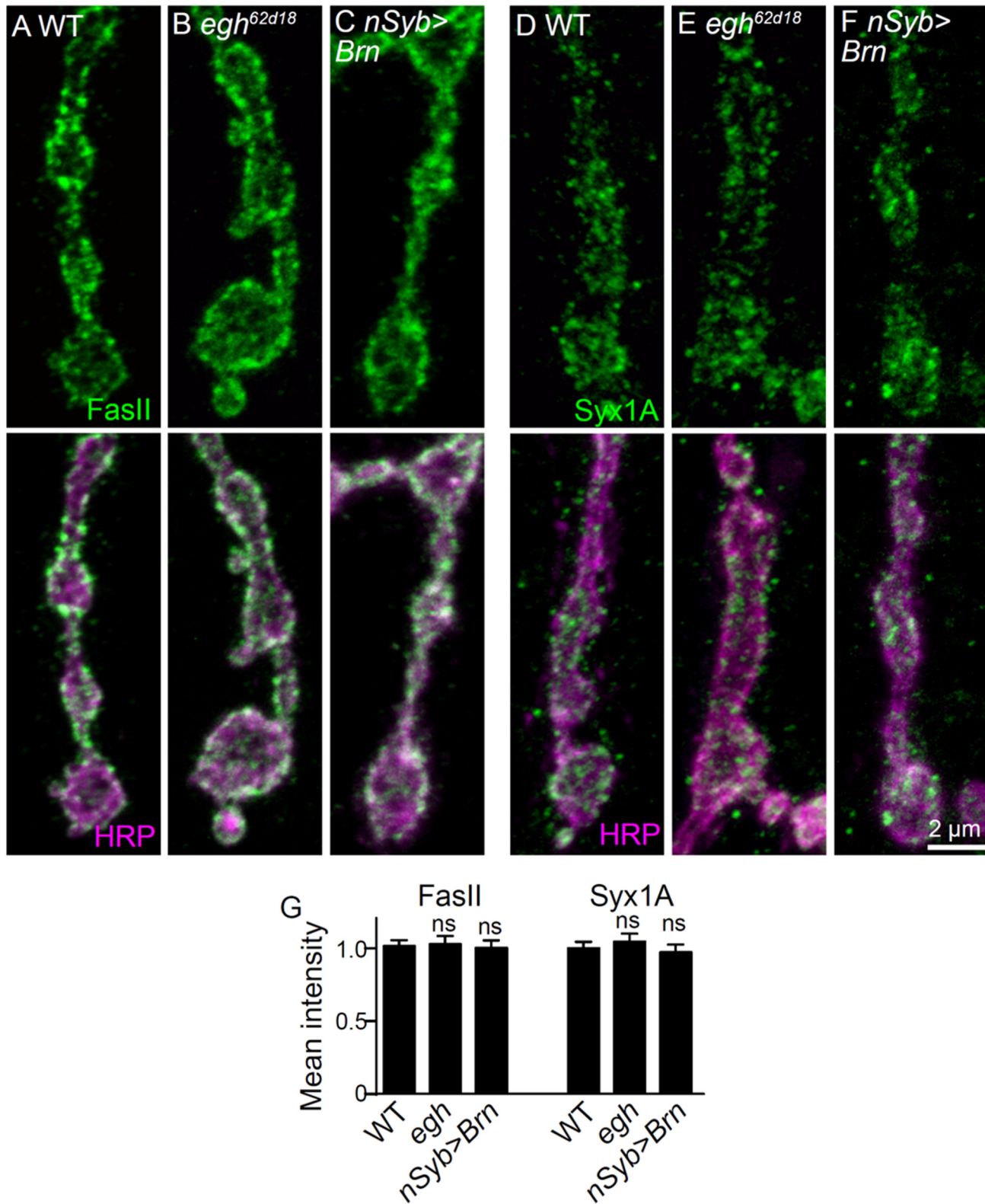
**Figure 2—figure supplement 2.** Alteration of *egh* and *brn* level in glia or muscle does not affect NMJ growth. (A–H) Images of NMJ4 co-stained with anti-HRP (green) and anti-CSP (magenta) in *UAS-Egh/+*; *C57-Gal4/+* (A), *egh<sup>62d18</sup>/Y*; *UAS-Egh/+*; *C57-Gal4/+* (B), *UAS-brn-RNAi/+*; *C57-Gal4/+* (C), *UAS-brn/C57-Gal4* (D), *UAS-Egh/+*; *Repo-Gal4/+* (E), *egh<sup>62d18</sup>/Y*; *UAS-Egh/+*; *Repo-Gal4/+* (F), *UAS-brn-RNAi/+*; *Repo-Gal4/+* (G) and *UAS-brn/Repo Gal4* (H). Scale bar: 10  $\mu$ m. (I) Quantifications of bouton number, satellite bouton number, and bouton size of NMJ4 from different genotypes. 'CT' denotes corresponding control in each multiple comparison. ns, no significance, \*\* $p < 0.01$ , \*\*\* $p < 0.001$  one-way ANOVA with Tukey post hoc tests;  $n \geq 12$  larvae; error bars: s.e.m.

DOI: <https://doi.org/10.7554/eLife.38183.005>



**Figure 3.** MacCer staining intensity at NMJs is bi-directionally regulated by Egh and Brn. (A) Images of wild-type NMJ4 co-stained with anti-MacCer (green), anti-HRP (blue) and anti-DLG (red). MacCer puncta were apparent in presynaptic boutons. Scale bar: 10  $\mu$ m. (B) Statistical results of normalized intensities of MacCer against anti-HRP staining within presynaptic boutons in different genotypes. \*\* $p < 0.01$  and \*\*\* $p < 0.001$  by student's *t* test between a test genotype and wild type;  $n \geq 16$  larvae; error bars: s.e.m. (C–H) Representative images of NMJ4 stained with anti-MacCer in wild type (C), *egh<sup>62d18</sup>/Y* (D), *UAS-Egh/+; nSyb-Gal4/+* (E), *brn<sup>1.6P6</sup>/brn<sup>fs107</sup>* (F), *UAS-brn-RNAi/+; nSyb-Gal4/+* (G) and *nSyb-Gal4/UAS-Brn* (H). Scale bar: 5  $\mu$ m.

DOI: <https://doi.org/10.7554/eLife.38183.007>



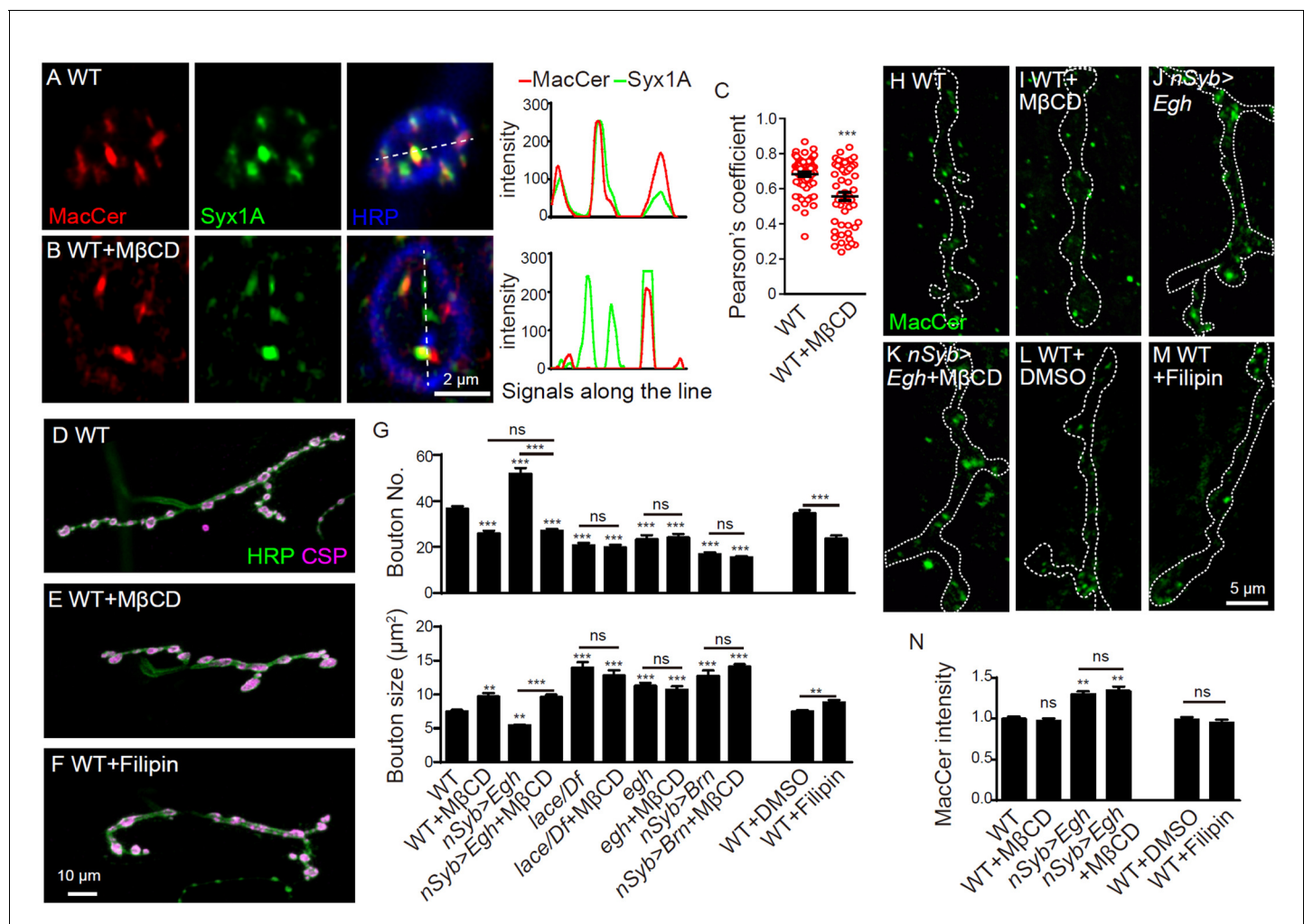
**Figure 3—figure supplement 1.** Images and quantifications of Fas II and Syx1A staining at NMJs of different genotypes. (A–C) Images of NMJ4 co-stained with anti-Fas II (green) and anti-HRP (magenta) in wild type, *egh*<sup>62d18</sup>/Y, and *nSyb-Gal4/UAS-brn*. (D–F) Images of NMJ4 co-stained with anti-Syx1A (green) and anti-HRP (magenta) in wild type, *egh*<sup>62d18</sup>/Y, and *nSyb-Gal4/UAS-brn*. (G) Quantification of mean intensity of Fas II and Syx1A staining. Error bars represent standard deviation. ns, not significant.



Figure 3—figure supplement 1 continued

Syx1A (green) and anti-HRP (magenta) in wild type, *egh<sup>62d18</sup>/Y*, and *nSyb-Gal4/UAS-brn*. Scale bar: 2  $\mu$ m. (G) Quantification of intensities of indicated markers normalized to HRP intensities in different genotypes.  $n \geq 10$  larvae; ns, no significance by student's t test; error bars: s.e.m.

DOI: <https://doi.org/10.7554/eLife.38183.008>



**Figure 4.** Sterol-depletion inhibits NMJ growth in a common genetic pathway with MacCer. (A and B) Confocal images of single slice of NMJ4 boutons triple-labeled with anti-MacCer (red), anti-Syx1A (green) and anti-HRP (blue) in wild type with or without 20 mM M $\beta$ CD treatment. Plot profiles of the relative intensity along the dashed lines are shown. (C) Pearson's coefficients of colocalization between MacCer and Syx1A.  $n = 63$  and  $52$  boutons from eight wild-type larvae each with or without M $\beta$ CD treatment. (D–F) Images of NMJ4 co-labeled for anti-HRP (green) and anti-CSP (magenta) in untreated wild type (D), wild type treated with 20 mM M $\beta$ CD (E), wild type treated with 50  $\mu$ g/ml filipin III (F), Scale bar: 10  $\mu$ m. (G) Quantification of bouton number and bouton size of NMJs. ns, no significance, \*\*\* $p < 0.001$  by one-way ANOVA with Tukey post hoc tests, error bars: s.e.m. (H–M) Images of NMJs from larvae stained with anti-MacCer of wild type (H), wild type treated with 20 mM M $\beta$ CD (I), *UAS-Egh/+; nSyb-Gal4/+* (J), and *UAS-Egh/+; nSyb-Gal4/+* treated with 20 mM M $\beta$ CD (K), wild-type larvae treated with vehicle DMSO (L) or 50  $\mu$ g/ml filipin III (M). Scale bar: 5  $\mu$ m. (N) Quantification of MacCer intensities normalized to HRP intensities in different genotypes. ns, no significance; \*\* $p < 0.01$  by one-way ANOVA with Tukey post hoc tests;  $n \geq 12$  larvae; error bars: s.e.m.

DOI: <https://doi.org/10.7554/eLife.38183.010>



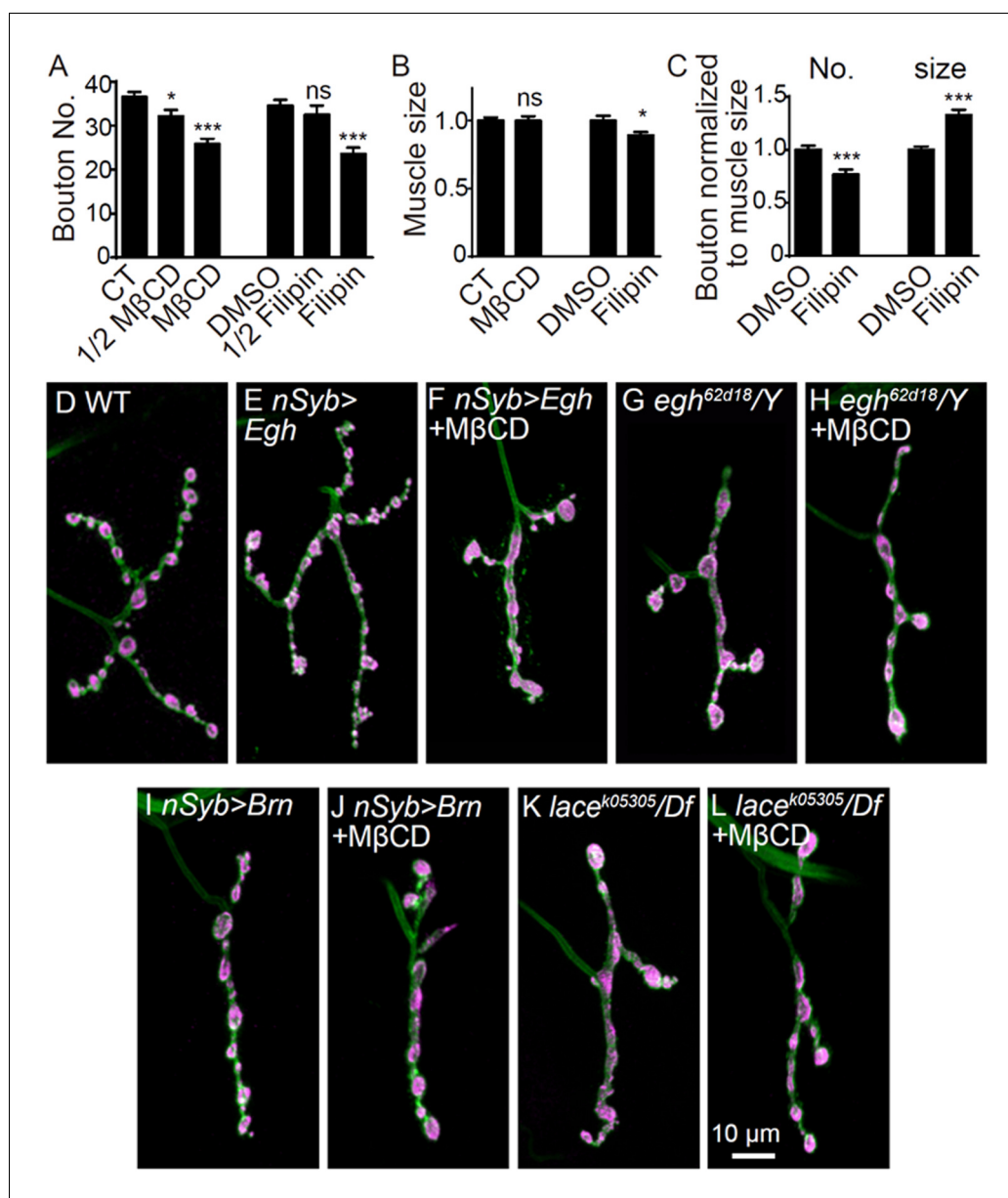


**Figure 4—figure supplement 1.** Additional NMJ images and quantifications of bouton number and bouton size. (A) Quantification of bouton number of NMJ4 from wild-type larvae fed with 0 mM (CT), 10 mM, 20 mM MβCD and 0 μg/ml (DMSO vehicle only), 25 μg/ml, 50 μg/ml filipin III. (B and C) Quantifications of muscle four surface area (B), relative bouton number and size normalized to muscle surface area (C) upon indicated treatments.  $n \geq 8$  larvae; ns, no significance, \* $p < 0.05$ , \*\*\* $p < 0.001$  by one-way ANOVA with Tukey *post hoc* tests; error bars: s.e.m. (D–L) Images of NMJ4 co-labeled for anti-HRP (green) and anti-CSP (magenta) in untreated wild type (D), *UAS-Egh/+; nSyb-Gal4/+* (E), *UAS-Egh/+; nSyb-Gal4/+* treated with 20 mM MβCD (F), *egh<sup>62d18</sup>/Y* (G), MβCD treated *egh<sup>62d18</sup>/Y* (H), *nSyb-Gal4/UAS-brn* (I), MβCD treated *nSyb-Gal4/UAS-brn* (J), *lace<sup>k05305</sup>/Df(2L)Exel7063* (K), and MβCD treated *lace<sup>k05305</sup>/Df(2L)Exel7063* (L). Scale bar: 10 μm.

DOI: <https://doi.org/10.7554/eLife.38183.011>

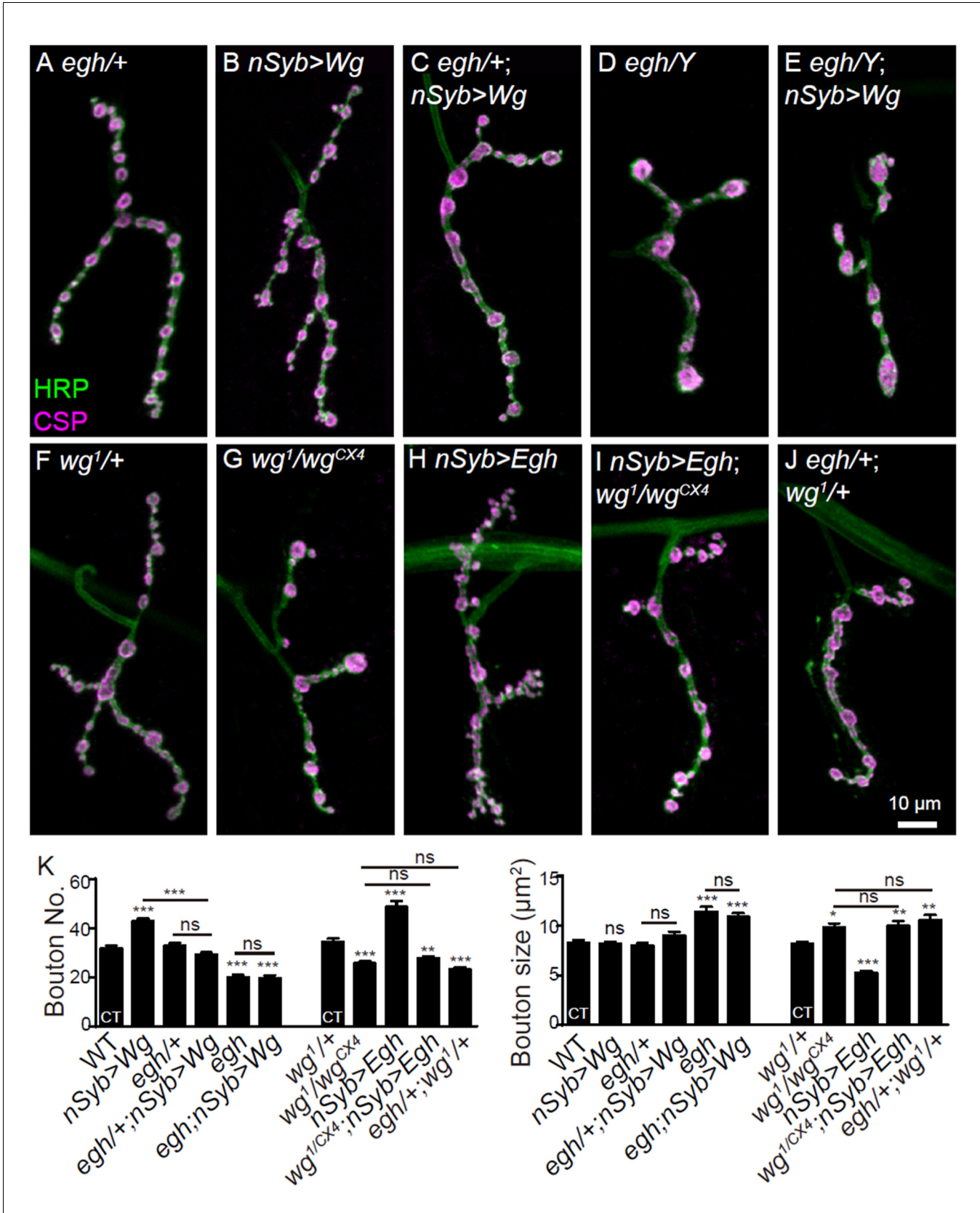


**Figure 5.** MacCer is required for the NMJ growth-promoting effect of Wg signaling. (A–J) Representative images of NMJ4 co-stained with anti-HRP (green) and anti-CSP (magenta) in *egh*<sup>62d18</sup>/+ (control, (A), *UAS-Wg-HA/+; nSyb-Gal4/+* (B), *egh*<sup>62d18</sup>/+; *UAS-Wg-HA/+; nSyb-Gal4/+* (C), *egh*<sup>62d18</sup> (D), Figure 5 continued on next page

Figure 5 continued

*egh*<sup>62d18</sup>; *UAS-Wg-HA*/+; *nSyb-Gal4*/+ (E), *wg*<sup>1</sup>/+ (F), *wg*<sup>1</sup>/*wg*<sup>CX4</sup> (G), *nSyb-Gal4*/*UAS-Egh* (H), *wg*<sup>CX4</sup>/*UAS-Egh*/*wg*<sup>1</sup>; *nSyb-Gal4*/+ (I), and *egh*<sup>62d18</sup>/+; *wg*<sup>1</sup>/+ (J). Scale bar: 10  $\mu$ m. (K) Quantifications of bouton number and bouton size of NMJs in different genotypes. 'CT' denotes corresponding control in each multiple comparison.  $n \geq 12$  larvae; ns, no significance, \* $p < 0.05$ ; \*\* $p < 0.01$ ; \*\*\* $p < 0.001$  by one-way ANOVA with Tukey *post hoc* tests, error bars: s.e.m.

DOI: <https://doi.org/10.7554/eLife.38183.013>

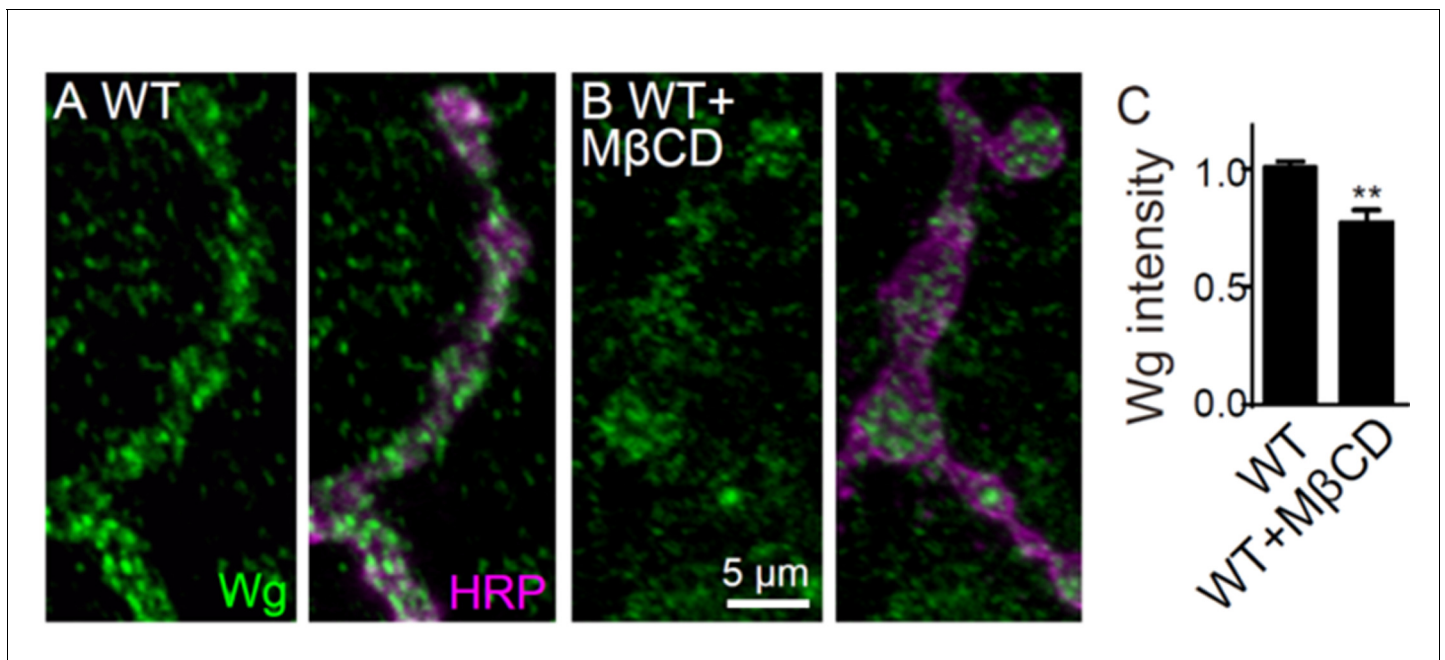


**Figure 5—figure supplement 1.** Additional NMJ images and quantifications. Images of NMJ4 co-labeled for anti-HRP (green) and anti-CSP (magenta) in *nSyb-Gal4/UAS-brn* (A), *UAS-Wg-HA/+; nSyb-Gal4/UAS-brn* (B), wild type treated with 20 mM MβCD (C), *UAS-Wg-HA/+; nSyb-Gal4/+* treated with 20 mM MβCD (D), *arr<sup>k0813</sup>/+* (E), *arr<sup>k0813</sup>/arr<sup>2</sup>* (F), *egh<sup>62d18</sup>/+*; *arr<sup>k0813</sup>/+* (G), *evi<sup>2</sup>/+* (H), *evi<sup>2</sup>* (I), and *egh<sup>62d18</sup>/+*; *evi<sup>2</sup>/+* (J). Scale bar: 10 μm. (K) Quantification of bouton number and bouton size of NMJs.  $n \geq 12$  larvae; ns, no significance, \* $p < 0.05$ ; \*\* $p < 0.01$  and \*\*\* $p < 0.001$  by one-way ANOVA with Tukey post hoc tests, error bars: s.e.m. (L and M) Representative images of NMJ4 co-labeled with anti-Wg (green) and anti-HRP (magenta) in wild type (L) and wild type treated with 20 mM MβCD (M). Scale bar: 5 μm. (N) Quantification of Wg intensity normalized to HRP intensity.  $n \geq 15$  larvae; ns, no significance; \*\* $p < 0.01$  by student's t test; error bars: s.e.m.

DOI: <https://doi.org/10.7554/eLife.38183.014>

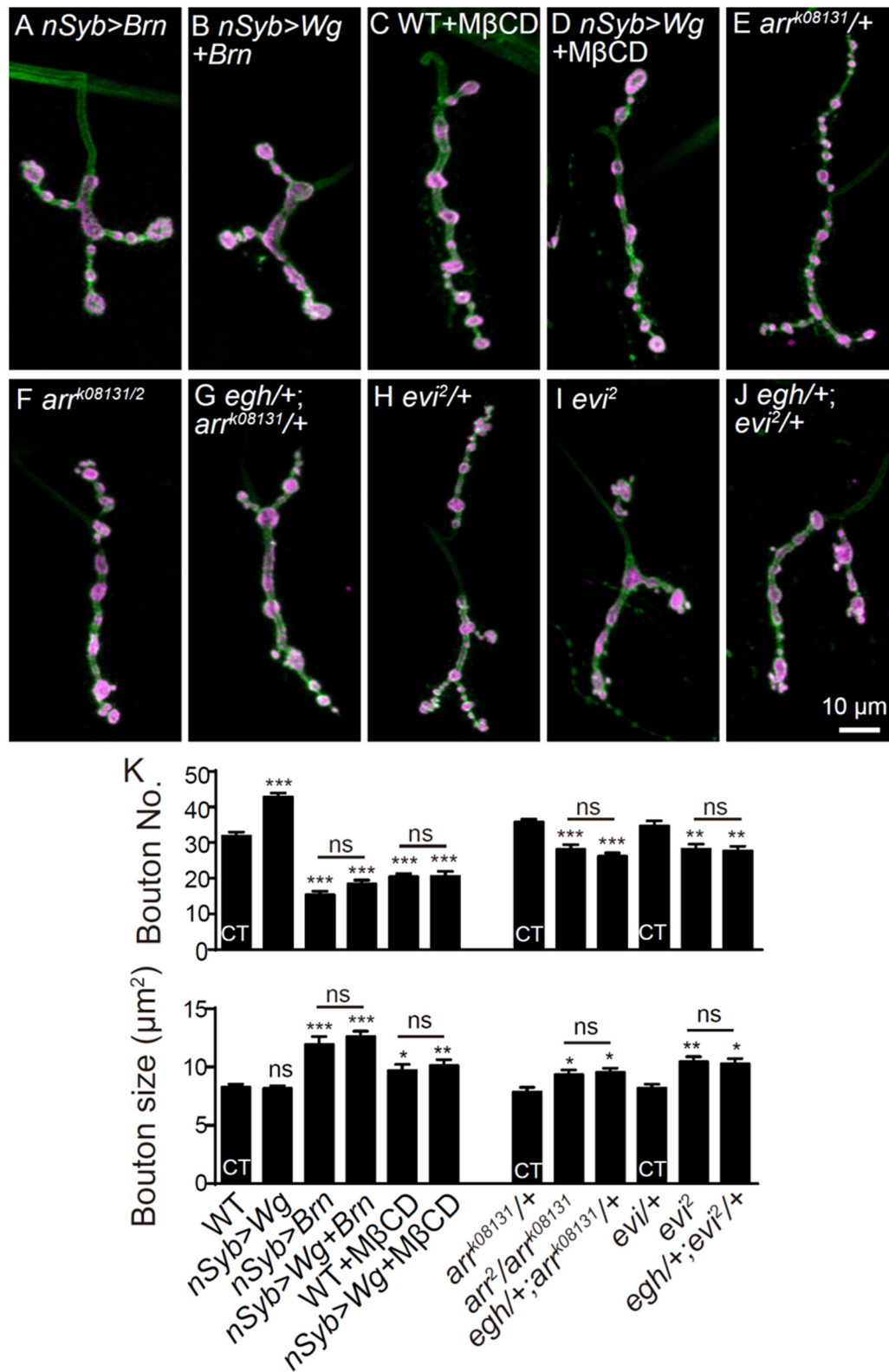


**Figure 5—figure supplement 2.** Additional NMJ images and quantifications.

DOI: <https://doi.org/10.7554/eLife.38183.015>



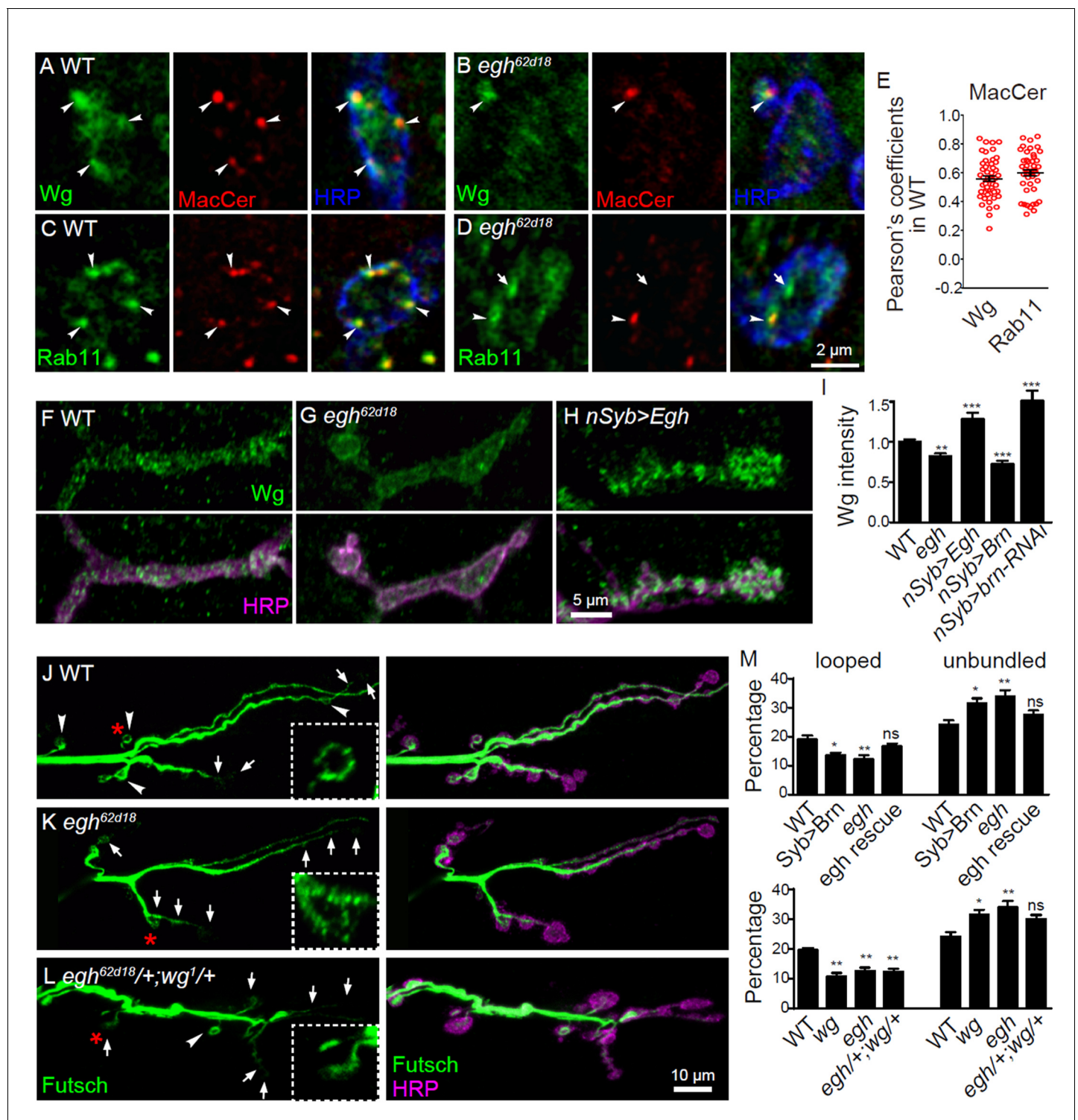


**Figure 6.** MacCer is required for the local presynaptic Wg signaling at NMJs. (A–D) Confocal images of single slice of NMJ4 boutons triple-labeled with anti-MacCer (red), anti-HRP (blue) and anti-Wg (green; A–B) or anti-Rab11 (green; C–D) in wild type and *egh*<sup>62d18</sup> mutants. MacCer puncta showed substantial colocalization (arrowheads) with Wg and Rab11 in boutons. Arrows indicate Rab11-positive puncta without MacCer staining in the *egh*<sup>62d18</sup> mutants. Images were processed by deconvolution. Scale bar: 2  $\mu$ m. (E) Pearson's coefficients of colocalization between MacCer and indicated proteins.  $n = 51$  and 44 boutons (from ten wild-type larvae each) for colocalization of MacCer with Wg and Rab11, respectively. (F–H) Representative images of NMJ4 co-labeled with anti-Wg (green) and anti-HRP (magenta) in wild type (F), *egh*<sup>62d18</sup> mutants (G) and *UAS-Egh/+; nSyb-Gal4/+* (H). Scale bar: 5  $\mu$ m. (I) Quantification of intensities of endogenous Wg normalized to HRP intensities in different genotypes.  $n \geq 15$  larvae; ns, no significance; \*\*\* $p < 0.001$ , \*\* $p < 0.01$ , \* $p < 0.05$ . (J–L) Confocal images of NMJ4 boutons triple-labeled with anti-Futsch (green), anti-HRP (magenta) and anti-Wg (green) in wild type (J), *egh*<sup>62d18</sup> mutants (K) and *egh*<sup>62d18/+; wg<sup>1/+</sup> (L). Scale bar: 10  $\mu$ m. (M) Quantification of the percentage of looped and unbundled NMJ4 boutons in different genotypes.  $n \geq 15$  larvae; ns, no significance; \*\*\* $p < 0.001$ , \*\* $p < 0.01$ , \* $p < 0.05$ .</sup>



## Figure 6 continued

\*\* $p < 0.01$  and \*\*\* $p < 0.001$  by student's  $t$  test; error bars: s.e.m. (J–L) Representative images of NMJ6/7 labeled with anti-Futsch (green) and anti-HRP (magenta) in wild type (J),  $egh^{62d18}$  mutants (K) and  $egh^{62d18}/+; wg^1/+$  transheterozygotes (L). Insets show higher magnification images of Futsch staining of a single bouton (asterisk). Arrows indicate boutons displaying unbundled Futsch; arrowheads denote boutons with Futsch loops. Scale bar: 10  $\mu\text{m}$ . (M) Quantifications of percentage of Futsch loops and unbundled Futsch staining in different genotypes. The genotype of  $egh$  rescue was  $egh^{62d18}; UAS-Egh/+; nSyb-Gal4/+$ ; the genotype of  $wg$  was  $wg^1/wg^{CX4}$ .  $n \geq 12$  larvae; ns, no significance, \* $p < 0.05$ ; \*\* $p < 0.01$  by one-way ANOVA with Tukey post hoc tests, error bars: s.e.m.

DOI: <https://doi.org/10.7554/eLife.38183.017>

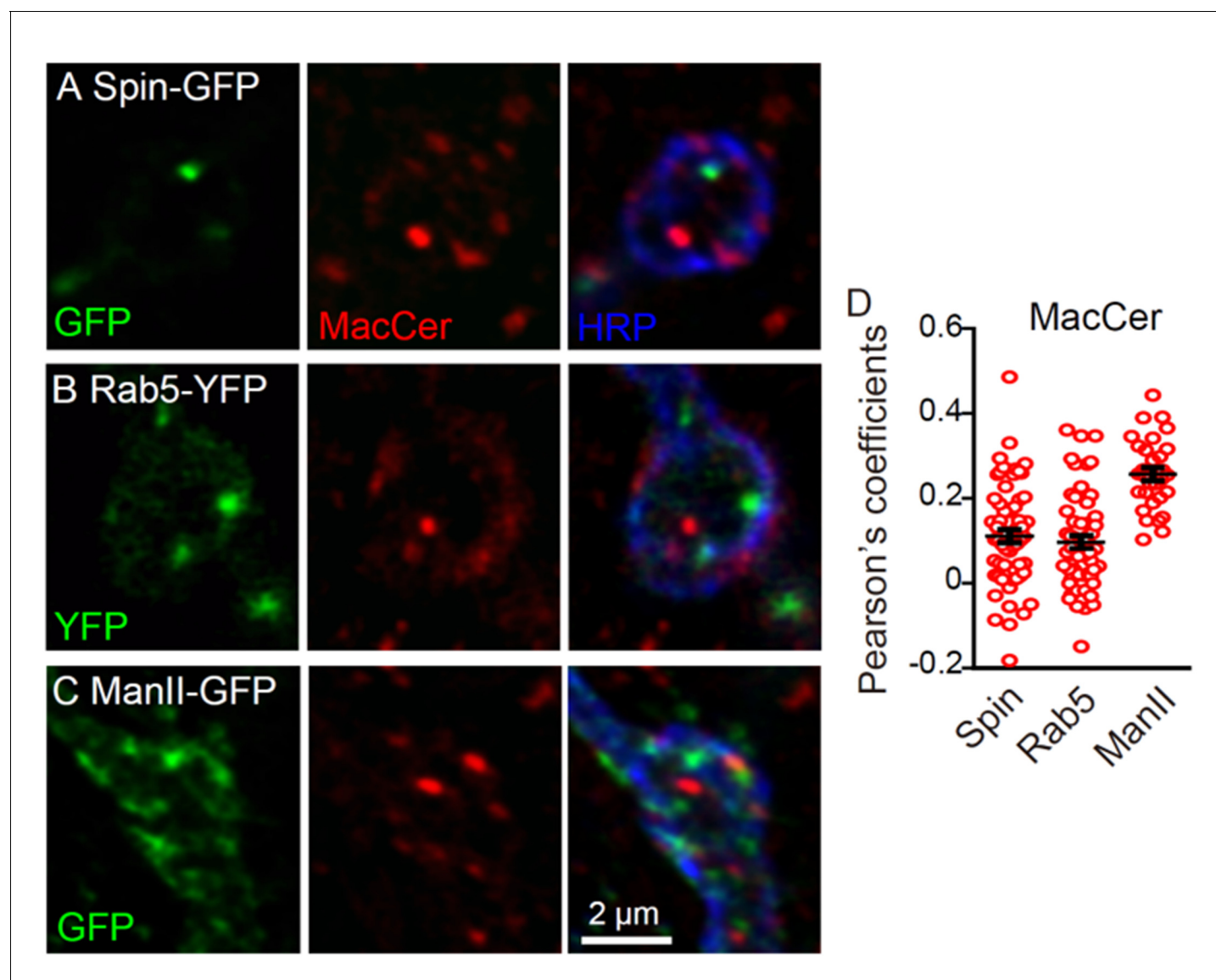


**Figure 6—figure supplement 1.** MacCer puncta showed few overlap with Rab5-YFP, Spintest-GFP and Mannose II-GFP. Single sections of NMJ4 boutons triple-labeled with anti-MacCer (red), anti-HRP (blue), and specific organelle markers (green) in *nSyb-Gal4/UAS-Spin-GFP* (A), *UAS-YFP-Rab5/+; nSyb-Gal4/+* (B), and *nSyb-Gal4/UAS-ManII-GFP* (C) larvae. MacCer puncta showed few overlaps with these organelles in NMJ boutons. Images were processed by deconvolution. Scale bar: 2  $\mu$ m. (D) Pearson's coefficients of colocalization between MacCer and indicated proteins.  $n = 61/9$ ,  $57/8$ , and  $30/5$  (from left to right, boutons/animals).

DOI: <https://doi.org/10.7554/eLife.38183.018>

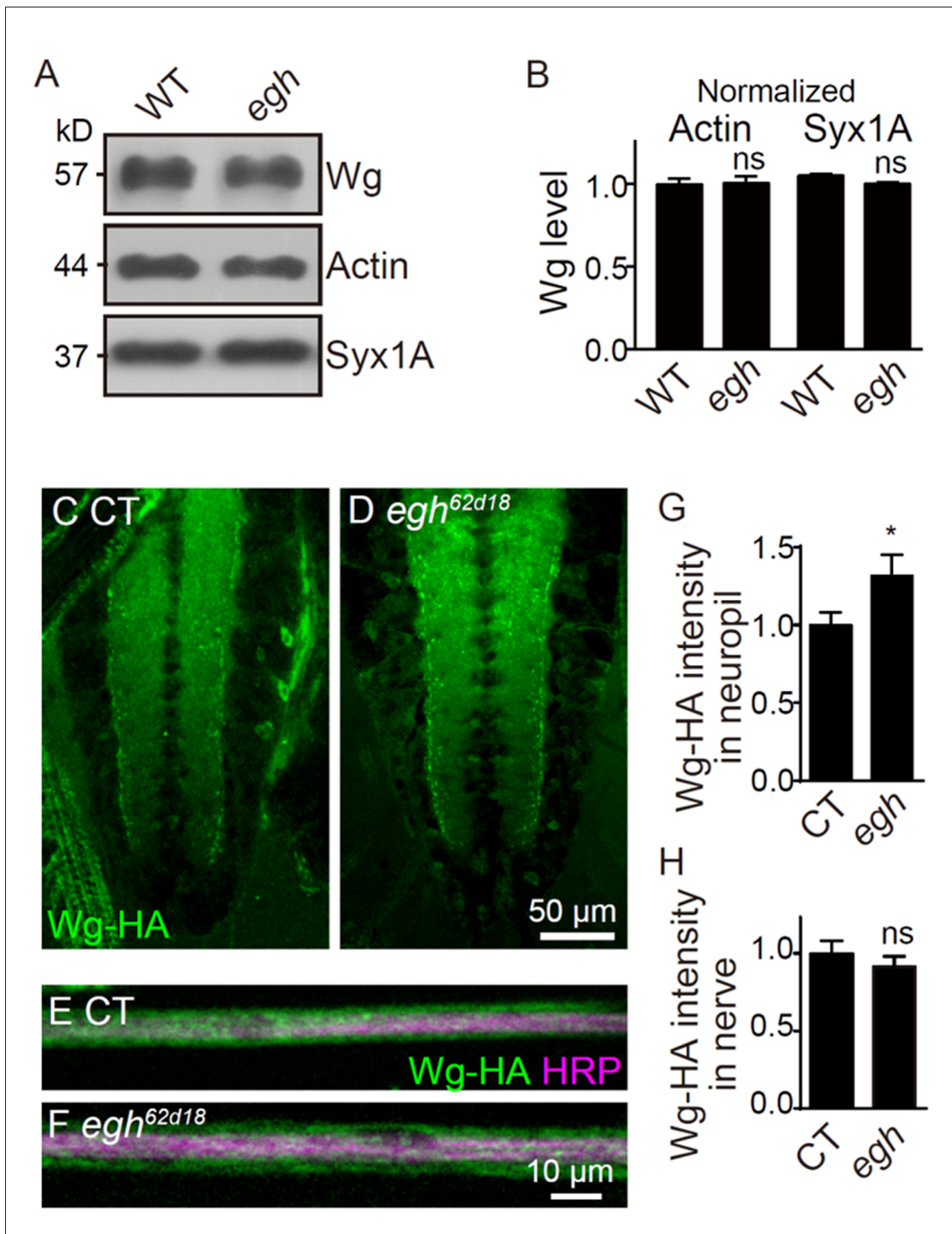
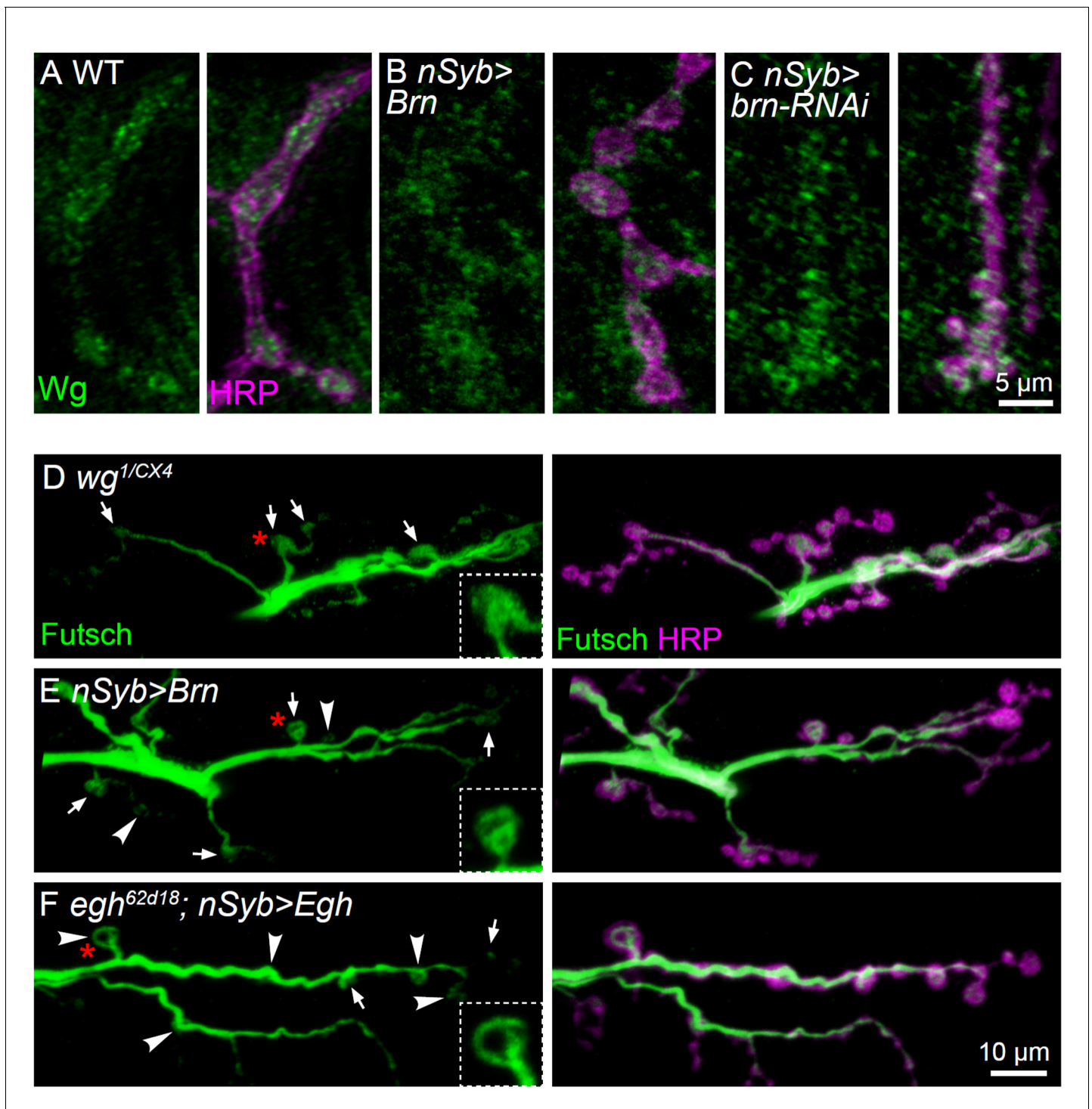


**Figure 6—figure supplement 2.** The Wg level in *egh* brains by immunochemical analysis. (A and B) Western blotting and quantification of Wg from 3rd instar larval brains of wild type and *egh*<sup>62d18</sup> mutants, normalized to the level of Actin and Syntaxin 1A (Syx1A).  $n = 3$ ; ns, no significance by one-way ANOVA. Figure 6—figure supplement 2 continued on next page

Figure 6—figure supplement 2 continued

ANOVA test; error bars: s.e.m. (C and D) Images of ventral nerve cord stained with anti-HA in *UAS-Wg-HA/+; nSyb-Gal4/+* (control, C) and *egh<sup>62d18</sup>/Y; UAS-Wg-HA/+; nSyb-Gal4/+* (D). Scale bar: 50  $\mu$ m. (E and F) Images of segmental nerve stained with anti-HA (green) and anti-HRP (magenta) in *UAS-Wg-HA/+; nSyb-Gal4/+* (control, E) and *egh<sup>62d18</sup>/Y; UAS-Wg-HA/+; nSyb-Gal4/+* (F). Scale bar: 10  $\mu$ m. (G and H) Quantifications of HA intensity in neuropils and segmental nerves of control and *egh* mutants.  $n \geq 8$  larvae; ns, no significance, \* $p < 0.05$  by student's *t* test; error bars: s.e.m.

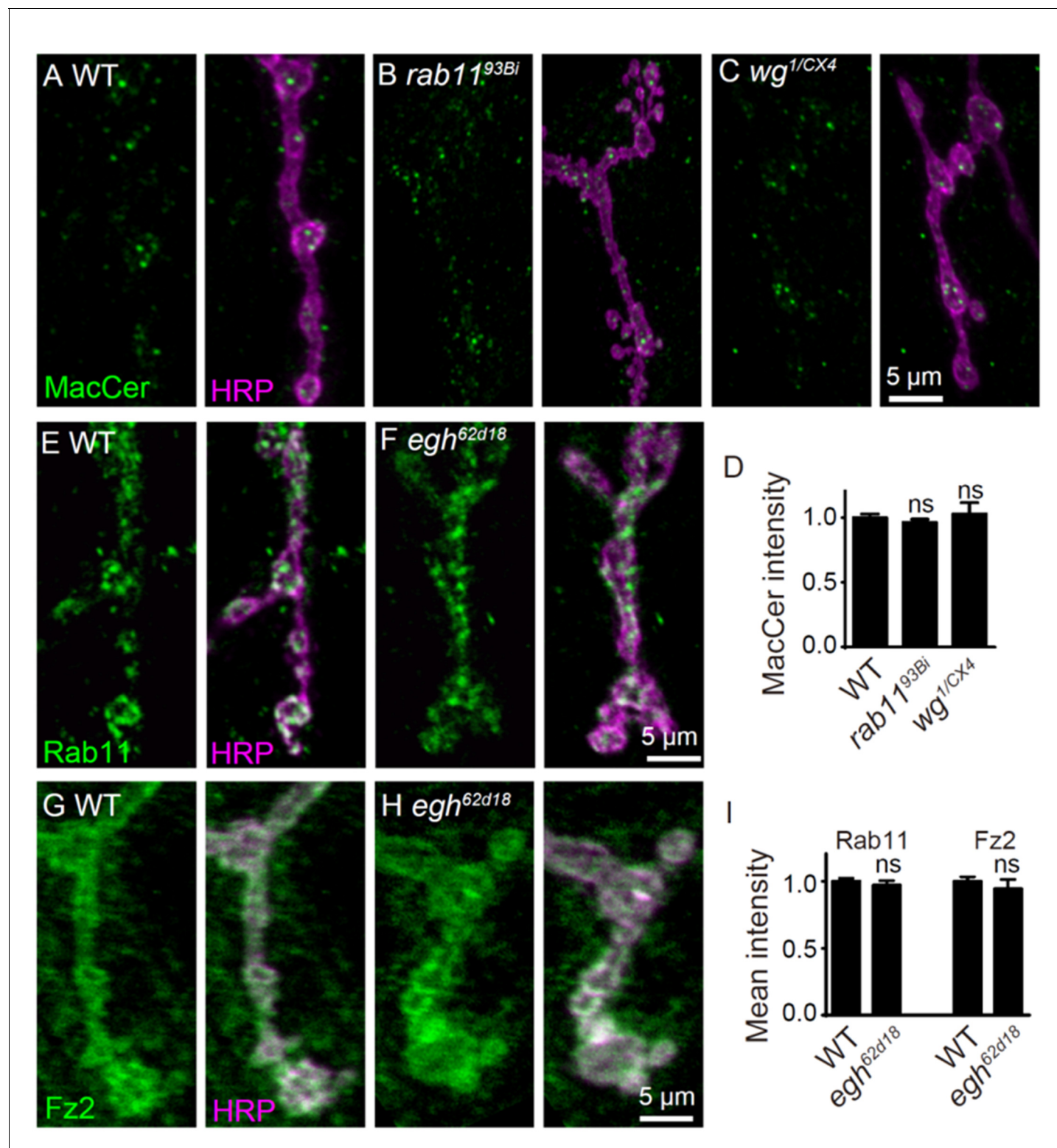
DOI: <https://doi.org/10.7554/eLife.38183.019>



**Figure 6—figure supplement 3.** Additional images showing Wg and Futsch staining at NMJ of different genotypes. (A–C) Representative images of NMJ4 co-labeled with anti-Wg (green) and anti-HRP (magenta) in wild type (A), *nSyb-Gal4/UAS-brn* (B) and *UAS-brn-RNAi/+; nSyb-Gal4/+* (C). Scale bar: 5  $\mu\text{m}$ . (D–F) Representative images of NMJ6/7 co-labeled with anti-Futsch (green) and anti-HRP (magenta) in *wg<sup>1/wg<sup>CX4</sup></sup>* (D), *nSyb-Gal4/UAS-Brn* (E), and *egh<sup>62d18</sup>/Y; UAS-Egh/+; nSyb-Gal4/+* (F). Insets show higher magnification images of Futsch staining of a single bouton (asterisk in red). Arrows indicate boutons displaying unbundled Futsch; arrowheads denote boutons with Futsch loops. Scale bar: 10  $\mu\text{m}$ .

DOI: <https://doi.org/10.7554/eLife.38183.020>

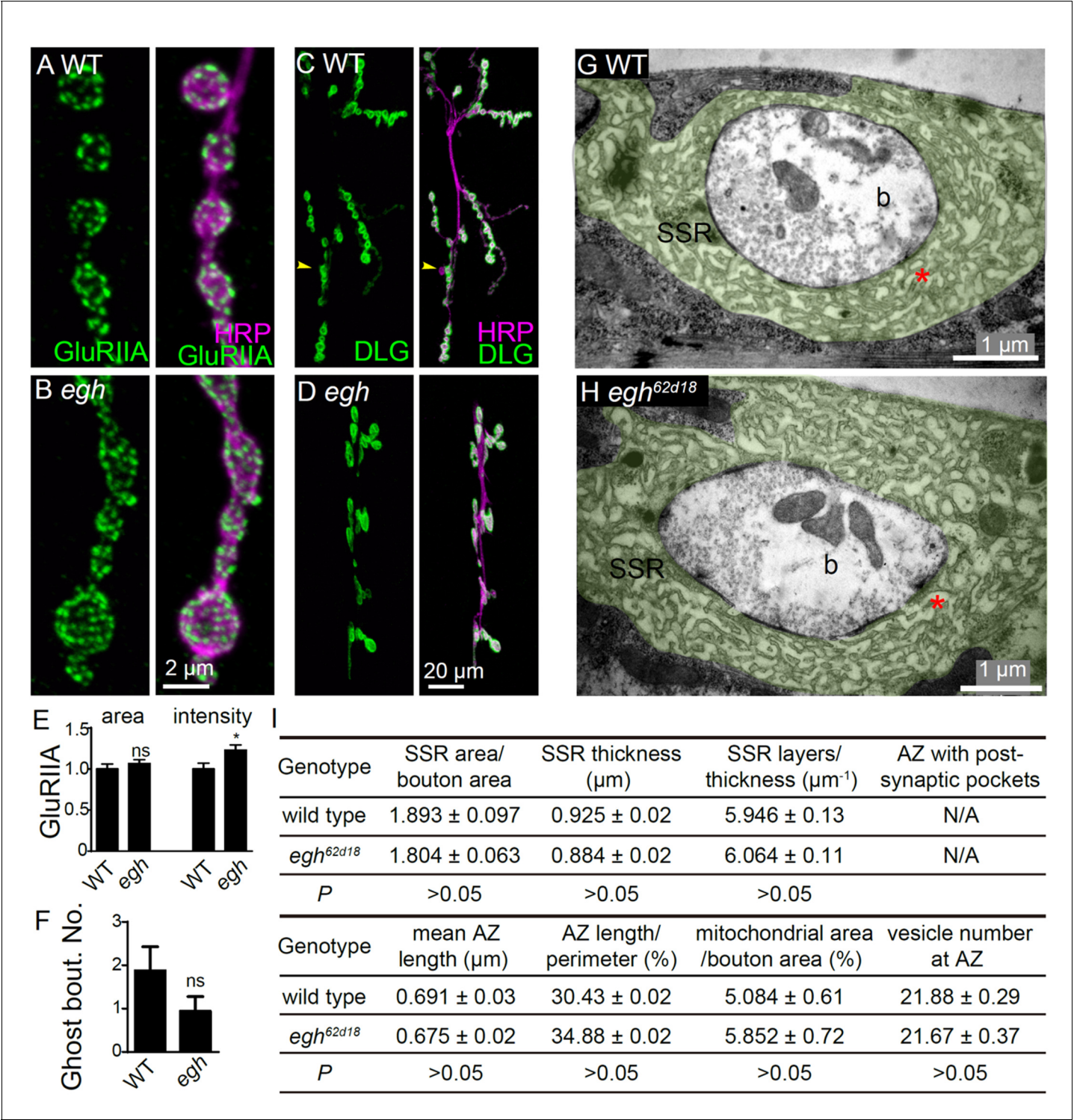




**Figure 6—figure supplement 4.** Images and quantifications of MacCer, Rab11, and Fz2 staining at NMJ of different genotypes. (A–C) Images of NMJ4 co-stained with anti-MacCer (green) and anti-HRP (magenta) in wild type (A), *rab11<sup>93Bi</sup>* (B) and *wg<sup>1/CX4</sup>* (C). (D) Quantification of MacCer intensity normalized to HRP intensity in different genotypes.  $n \geq 12$  larvae; ns, no significance by student's *t* test; error bars: s.e.m. (E–H) Images of NMJ4 co-stained with anti-Rab11 or anti-Fz2 (green) and anti-HRP (magenta) in wild type and *egh<sup>62d18</sup>* mutants. (I) Quantification of synaptic intensities of Rab11 and Fz2 normalized to HRP intensities in different genotypes.  $n \geq 12$  larvae;  $p > 0.05$  by student's *t* test; error bars: s.e.m.

DOI: <https://doi.org/10.7554/eLife.38183.021>





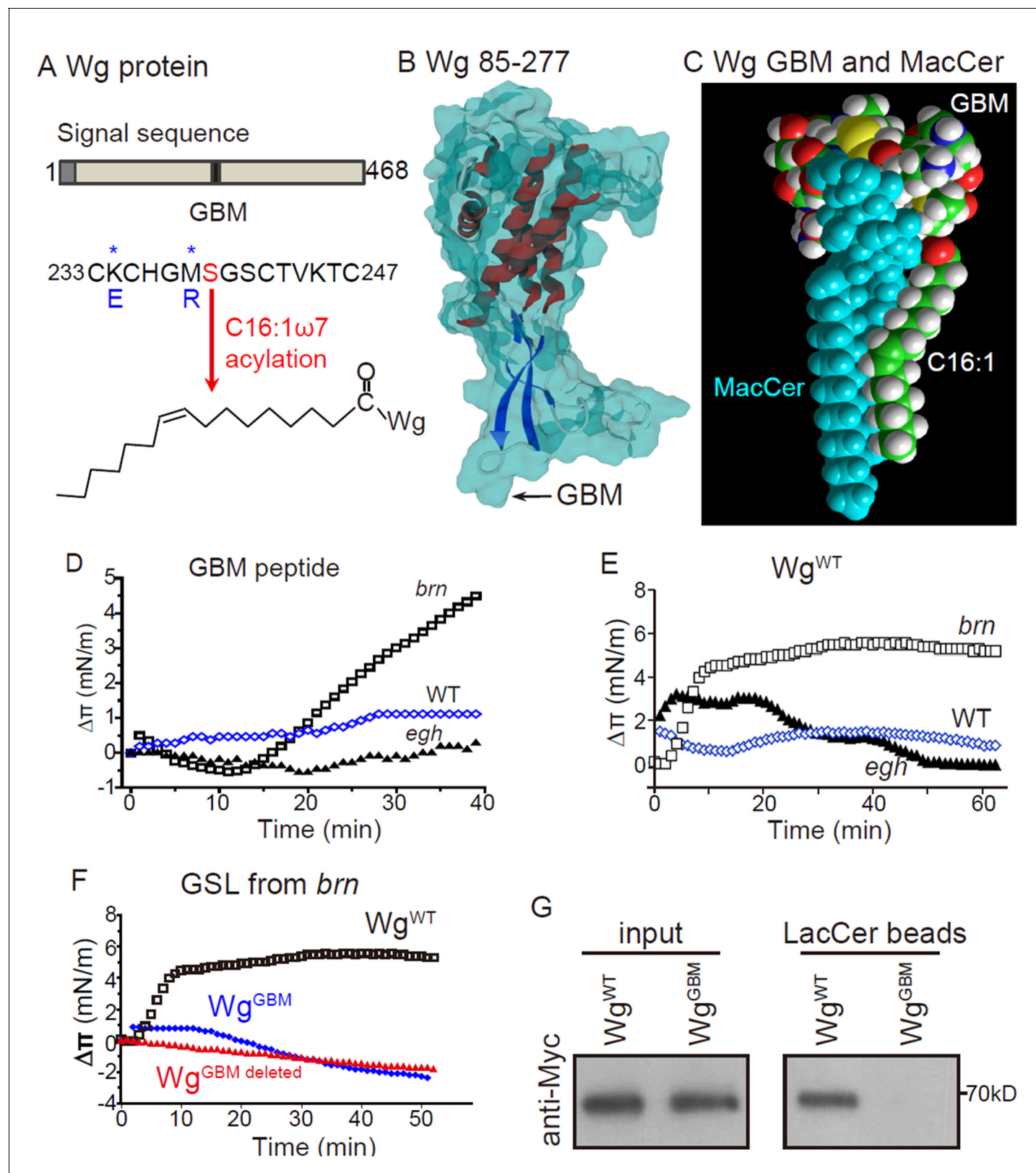
**Figure 7.** Postsynaptic differentiation is normal in *egh* mutants. (A and B) Representative images of NMJ4 from wild type and *egh*<sup>62d18</sup> mutants co-stained with anti-HRP (magenta) and anti-GluRIIA (green). Scale bar: 2 μm. (C and D) Images of NMJ6/7 from wild type and *egh*<sup>62d18</sup> mutants co-stained with anti-HRP (magenta) and anti-DLG (green). An arrowhead points at a ghost bouton. Scale bar: 20 μm. (E and F) Quantification of normalized intensities and area of GluRIIA against anti-HRP staining of NMJ4 (E) and ghost bouton number of NMJ6/7 (F) in wild type and *egh*<sup>62d18</sup> mutants. ns, no significance, \**p*<0.05 by student's *t* test; *n* ≥ 12 larvae; error bars: s.e.m. (G and H) Ultrastructure images of NMJ6/7 boutons from wild type and *egh*<sup>62d18</sup> mutants. The subsynaptic reticulum (SSR; green) is folded membrane network that surrounds the presynaptic bouton (b); The SSR region juxtaposed to the active zone (AZ) is indicated by asterisks in red. Scale bar: 1 μm. (I) Quantification of various bouton parameters of NMJ 6/7 synapses

Figure 7 continued on next page

Figure 7 continued

in wild type and *egh*<sup>62d18</sup> mutants. n = 50 boutons from five wild-type animals, and n = 37 boutons from three *egh*<sup>62d18</sup> larvae. Statistical analysis was performed by student's t test.

DOI: <https://doi.org/10.7554/eLife.38183.023>



**Figure 8.** Wg has a functional MacCer-binding domain (A) Schematic representation of Wg protein and amino acid sequence of a putative GSL-binding motif (GBM) and mutated GBM with asterisks denoting the mutated amino acids. (B) A 3D model of Wg residues 85–277 with the location of the GBM, which exposes on the protein surface. (C) Energy-minimized model of the acylated (C16:1  $\omega$ 7) GBM in Wg binding with MacCer. (D and E) Figure 8 continued on next page

## Figure 8 continued

Surface pressure change ( $\Delta\pi$ ) by the addition of Wg<sup>233-247</sup> peptide (GBM peptide; **D**) and full-length Wg produced by in vitro translation system (**E**) on a monolayer of GSLs purified from wild type, *egh*<sup>62d18</sup> and *brn*<sup>1.6P6</sup> larvae. GBM peptide and full-length Wg showed specific high affinity to MacCer enriched GSLs. (**F**) Surface pressure change ( $\Delta\pi$ ) by the addition of Myc-tagged wild-type Wg (Wg<sup>WT</sup>) and Wg with GBM deleted (Wg<sup>GBM deleted</sup>) or mutated (Wg<sup>GBM</sup>) on a monolayer of GSLs purified from *brn*<sup>1.6P6</sup> larvae. All surface pressure measurements were performed in triplicate and a representative curve is shown. (**G**) Wild-type Wg (Wg<sup>WT</sup>) but not Wg with mutated GBM (Wg<sup>GBM</sup>) was pulled-down by LacCer-beads. Five biological repeats were carried out for the pull-down assay and a representative blot is shown.

DOI: <https://doi.org/10.7554/eLife.38183.025>

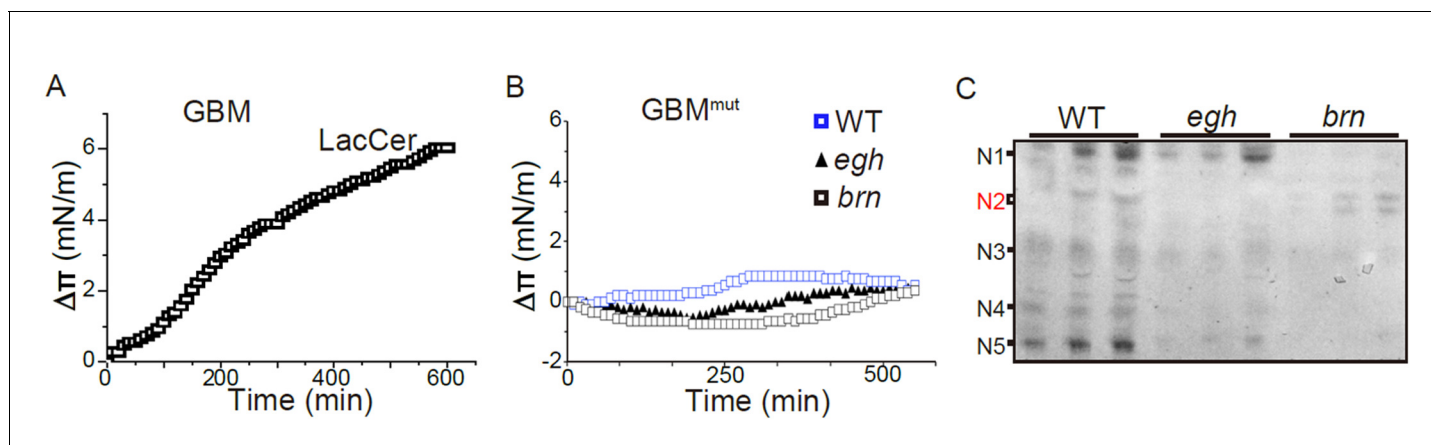


**Figure 8—figure supplement 1.** Additional monolayer data and GSL profiles of *egh* and *brn* mutants. (A) Surface pressure increase ( $\Delta\pi$ ) by the addition of the Wg<sup>233-247</sup> (GBM) peptide on a monolayer of LacCer. A maximal value was reached after 1 hr of incubation. (B) Surface pressure change ( $\Delta\pi$ ) by the addition of mutated GBM at Lys and Met ( $GBM^{mut}$ ) on a monolayer of GSLs purified from wild type, *egh*<sup>62d18</sup> and *brn*<sup>1.6P6</sup> larvae. All surface pressure measurements were performed in triplicate and a representative curve is shown. (C) GSL profile of wild type, *egh*<sup>62d18</sup> and *brn*<sup>1.6P6</sup> extracts (Ceramide mono-, di-, tri-, tetra- and penta-hexoside are denoted as N1, N2, N3, N4 and N5, respectively). Wild-type larvae express a broad range of GSLs including tetra- and penta-hexosylceramides, while *egh*<sup>62d18</sup> mutants lacked MacCer and *brn*<sup>1.6P6</sup> mutants contained almost exclusively MacCer (N2).

DOI: <https://doi.org/10.7554/eLife.38183.026>



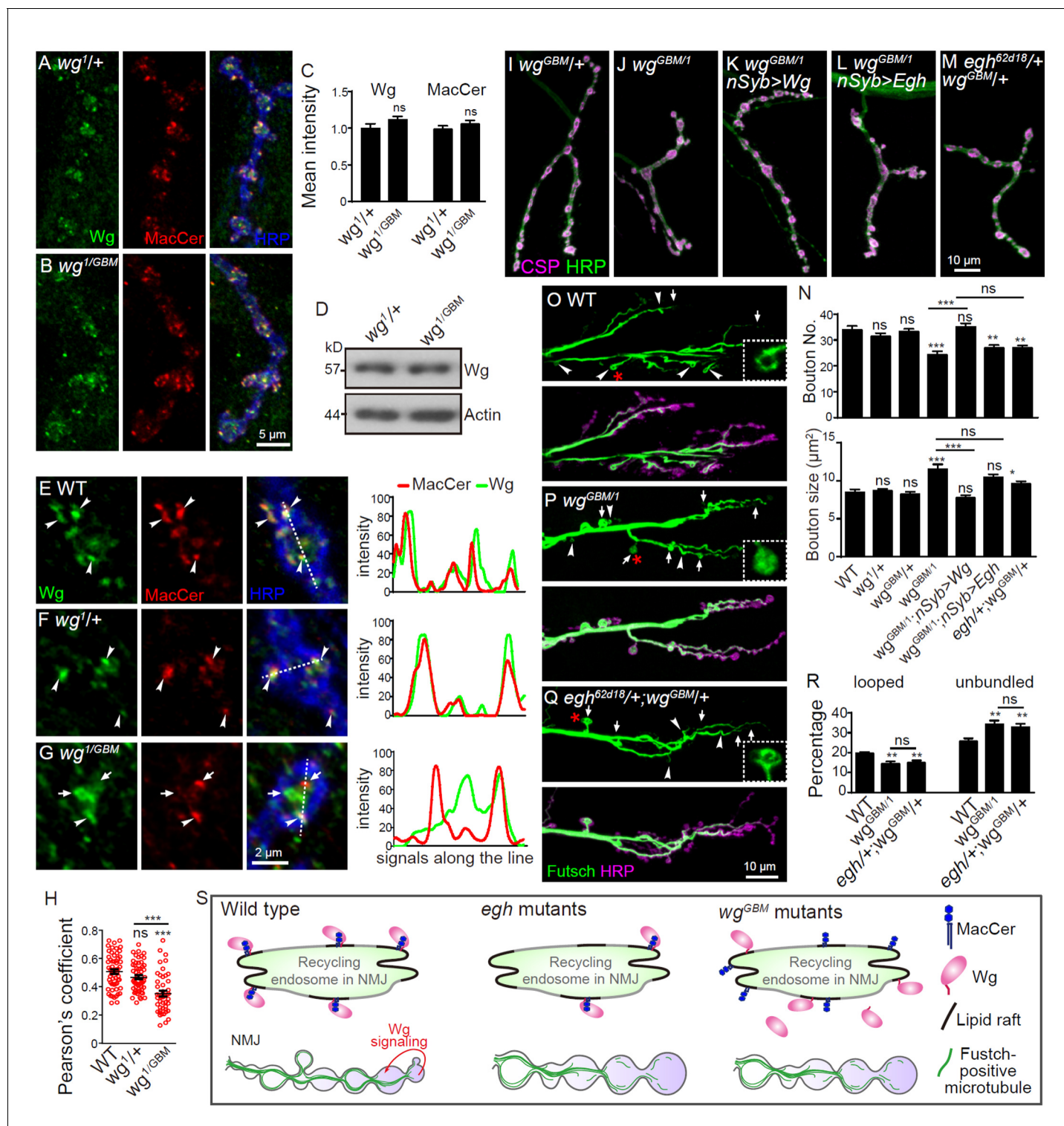


**Figure 9.** Wg GBM is required for Wg-MacCer colocalization and NMJ growth. (A and B) Representative images of NMJ4 co-labeled with anti-Wg (green), anti-MacCer (red) and anti-HRP (blue) in *wg<sup>1/+</sup>* (A) and *wg<sup>GBM/wg<sup>1</sup></sup>* mutants (B). (C) Quantification of Wg and MacCer intensities normalized to HRP intensities in different genotypes.  $n \geq 15$  larvae; ns, no significance by one-way ANOVA with Tukey post hoc tests; error bars: s.e.m. (D) Western results of Wg and Actin from 3rd instar larvae of *wg<sup>1/+</sup>* and *wg<sup>GBM/wg<sup>1</sup></sup>* mutants. Actin was used as a loading control. Western blots were performed in triplicate and a representative image is shown. (E–G) Representative images of NMJ4 boutons triple-labeled with anti-Wg (green), anti-MacCer (red) and anti-HRP (blue) in wild type (E), *wg<sup>1/+</sup>* (F) and *wg<sup>GBM/wg<sup>1</sup></sup>* mutants (G). Arrowheads indicate puncta positive for both MacCer and Wg signals; arrows indicate puncta without obvious overlap of MacCer and Wg. Images were processed by deconvolution. Scale bar: 2  $\mu$ m. Plot profiles of relative

## Figure 9 continued

intensity of MacCer and Wg along the dashed lines were shown. (H) Pearson's coefficients of colocalization between MacCer and Wg.  $n = 58/10, 57/8$ , and  $46/8$  (from left to right, boutons/animals). ns, no significance, \*\*\* $p < 0.001$  by one-way ANOVA with Tukey *post hoc* tests; error bars: s.e.m. (I–M) Representative images of NMJ4 co-stained with anti-HRP (green) and anti-CSP (magenta) in  $wg^{GBM}/+$  (I),  $wg^{GBM}/wg^1$  (J),  $UAS-Wg-HA, wg^{GBM}/wg^1; nSyb-Gal4/+$  (K),  $UAS-Egh, wg^{GBM}/wg^1; nSyb-Gal4/+$  (L), and  $egh^{62d18}/+; wg^{GBM}/+$  (M). Scale bar:  $10\ \mu\text{m}$ . (N) Quantifications of bouton number and bouton size of NMJs in different genotypes.  $n \geq 12$  larvae; ns, no significance, \* $p < 0.05$ ; \*\* $p < 0.01$ ; \*\*\* $p < 0.001$  by one-way ANOVA with Tukey *post hoc* tests, error bars: s.e.m. (O–Q) Representative images of NMJ6/7 labeled with anti-Futsch (green) and anti-HRP (magenta) in wild type (O),  $wg^{GBM}/wg^1$  (P), and  $egh^{62d18}/+; wg^{GBM}/+$  transheterozygotes (Q). Insets show higher magnification images of Futsch staining of a single bouton (asterisk). Arrows indicate boutons displaying unbundled Futsch; arrowheads denote boutons with Futsch loops. Scale bar:  $10\ \mu\text{m}$ . (R) Quantifications of percentage of Futsch loops and unbundled Futsch staining in different genotypes.  $n \geq 12$  larvae; ns, no significance, \*\* $p < 0.01$  by one-way ANOVA with Tukey *post hoc* tests, error bars: s.e.m. (S) A schematic presentation of the role for MacCer in promoting synapse growth via interacting with Wg in lipid rafts. The presynaptic Wg signaling is denoted by a curved arrow.

DOI: <https://doi.org/10.7554/eLife.38183.027>